

Inelastic Collisions of Fast Charged Particles with Atoms: Ionization of the Aluminum L Shell

Steven Trent Manson

Department of Physics, Georgia State University, Atlanta, Georgia 30303

(Received 17 April 1972)

Born-approximation calculations of the ionization of aluminum L -shell electrons have been performed using Hartree-Slater wave functions. Generalized oscillator strengths and proton energy-loss cross sections from threshold to ionized-electron energies of 128 Ry have been calculated. The results show a delayed maximum above threshold, and the ramifications of this phenomenon are discussed. Comparison is made with hydrogenic results and good agreement is found at intermediate and large energy loss, but the hydrogenic calculation is totally inadequate near threshold. The implications of this for stopping-power calculations and subshell corrections is discussed. The Bethe asymptotic cross section is obtained and the variation of parameters therein is investigated.

I. INTRODUCTION

The ionization of atoms by charged particles is a process of great importance in connection with plasma physics, space, atmospheric and astrophysics, and radiation physics. It is also the primary mechanism for energy loss of charged particles in matter. For sufficiently energetic particles the Born approximation adequately describes the ionization process^{1,2}; its accuracy is limited by the deficiencies in the wave functions employed for the initial and final states of the target atom.³ Many calculations of ionization cross sections using the Born approximation appear in the literature,⁴ but most use simple hydrogenic initial states. While this approach is probably valid for ionization of the K shell, it is expected to be unrealistic for L -shell ionization and even worse for outer shells, particularly for low ionized-electron energies. For example, experimental photoionization cross sections do not generally show the characteristic monotonic decrease above threshold, for L shell and higher, which is typical of the behavior of K -shell and hydrogenic results.⁵ This indicates that more realistic wave functions are needed for such calculations.

In this paper results are presented for the ionization of the L shell ($2s$ and $2p$) of aluminum. We use a nonrelativistic Hartree-Slater⁶ central-field model of the atom which has proved to be very useful in predicting photoionization cross sections.⁷⁻⁹ These calculations are performed for two primary aims: First, they are performed to provide reasonably reliable energy-loss cross sections in the ionized continuum, where very little experimental data exists. These results will then serve to give some insight into the total ionization cross section and stopping power. Second, they are performed to determine in which energy ranges the very much simpler hydrogenic calcula-

tion¹⁰⁻¹² provides a good approximation and where it fails. This information could then be used to calculate more accurate subshell corrections in the Bethe stopping-power theory.¹³⁻¹⁵

Quite recently a study using almost the same model as ours has been made by McGuire.¹⁶ This work complements ours, since McGuire is chiefly interested in total ionization cross sections for low- Z atoms, while we are mainly concerned with energy-loss cross sections for individual subshells in higher- Z elements.

II. THEORY

The cross section for the inelastic excitation or ionization of an atom or molecule from an initial state 0 to a final state η by particles of charge ze and velocity \tilde{v} is given in the (first) Born approximation by¹⁷

$$\sigma_{0\eta} = \frac{8\pi a_0^2 z^2}{m v^2 \mathcal{R}} \int_{K_{\min}}^{K_{\max}} \frac{|F_{0\eta}(K)|^2}{(Ka_0)^2} d \ln(Ka_0)^2, \quad (1)$$

where a_0 is the Bohr radius, m is the electron mass, \mathcal{R} is the Rydberg energy, and $\hbar \vec{K}$ is the momentum transfer. The inelastic scattering form factor $F_{0\eta}(K)$ is defined as

$$F_{0\eta}(K) = \langle \eta | \sum_j e^{i\vec{k} \cdot \vec{r}_j} | 0 \rangle, \quad (2)$$

with \vec{r}_j being the position vector of the j th electron of the target and the wave functions for discrete states normalized to unity; continuum functions per unit energy in rydbergs. The limits of integration in Eq. (1) can be obtained from the relation between the momentum transfer and θ the angle between the initial and final directions of the incident particle

$$(Ka_0)^2 = \frac{M}{m} \left\{ 2 \frac{T}{\mathcal{R}} - \frac{\Delta E}{\mathcal{R}} - 2 \left[\frac{T}{\mathcal{R}} \left(\frac{T}{\mathcal{R}} - \frac{\Delta E}{\mathcal{R}} \right) \right]^{1/2} \cos \theta \right\}, \quad (3)$$

where $\Delta E (= E_\eta - E_0)$ is the energy loss, M is the

incident particle mass, and $T(= \frac{1}{2}Mv^2)$ its kinetic energy. The minimum momentum transfer occurs when the incident particle does not change direction ($\theta = 0$) and the maximum occurs for back scattering ($\theta = \pi$). Note, however, that at very high energies this relation must be modified to take account of relativistic kinematics as discussed in Sec. 2.3 of Ref. 2. Furthermore, while the above definition of T remains unchanged in the relativistic region, it can no longer be identified with the kinetic energy.

Of great current interest is the generalized oscillator strength (GOS), which is defined as¹⁸

$$f_{0\eta}(K) = (E_\eta - E_0) (Ka_0)^{-2} |F_{0\eta}(K)|^2. \quad (4)$$

In terms of the GOS, the cross section can be expressed as

$$\sigma_{0\eta} = \frac{4\pi a_0^2 z^2}{T/\mathcal{R}} \frac{M}{m E_\eta - E_0} \frac{1}{\int_{K_{\min}}^{K_{\max}}} f_{0\eta}(K) d \ln(Ka_0)^2. \quad (5)$$

It is then clear, from Eq. (5), that the cross section is just proportional to the area under the $f_{0\eta}(K)$ -vs- $\ln(Ka_0)^2$ curve from K_{\min} to K_{\max} .¹⁸

In our calculations, we have employed wave functions which are products of one-electron orbitals. The one-electron functions $P_{nl}(r)$ for the initial ground state of the atom are of the Hartree-Slater⁶ type as tabulated by HS.¹⁹ Each of these functions, $P_{nl}(r)$, is a solution to the radial Schrödinger equation with the same central potential $V(r)$,

$$\left(\frac{d^2}{dr^2} + V(r) + \epsilon_{nl} - \frac{l(l+1)}{r^2} \right) P_{nl}(r) = 0, \quad (6)$$

$$V(r) \rightarrow 2Z/r \text{ as } r \rightarrow 0, \quad V(r) \rightarrow 2/r \text{ as } r \rightarrow \infty.$$

Here Z is the nuclear charge, ϵ_{nl} is the energy of an electron in the nl th subshell in rydbergs, and r is in units of $a_0 (= 5.29 \times 10^{-9} \text{ cm})$.

If an ionization process occurs in which an electron in the nl th subshell goes to a continuum $\epsilon l'$ state, we take this final-state orbital $P_{\epsilon l'}(r)$ to be the solution to the radial Schrödinger equation with the same central potential as the initial state

$$\left(\frac{d^2}{dr^2} + V(r) + \epsilon - \frac{l'(l'+1)}{r^2} \right) P_{\epsilon l'}(r) = 0, \quad (7)$$

in which ϵ is the ionized-electron energy in rydbergs and $P_{\epsilon l'}$ is normalized such that

$$P_{\epsilon l'}(r) \rightarrow \pi^{-1/2} \epsilon^{-1/4} \sin[\epsilon^{1/2} r - \epsilon^{-1/2} \ln 2 \epsilon^{1/2} r - \frac{1}{2} l' \pi + \sigma_{l'}(\epsilon) + \delta_{l'}(\epsilon)], \quad (8)$$

where

$$\sigma_{l'} = \arg \Gamma(l' + 1 - i \epsilon^{-1/2})$$

and $\delta_{l'}$ is the phase shift. This is the usual normalization of continuum wave functions per unit

energy range. The orbitals of the electrons not involved in the transition are taken to be unchanged from the initial state, i. e., we consider no core relaxation. The details of the numerical methods used to obtain and normalize the continuum wave functions are given in Refs. 7 and 8.

In order to carry out the integration of the form factor [Eq. (2)] we use the well-known expansion

$$e^{i\vec{k} \cdot \vec{r}} = \sum_{\lambda} (i)^{\lambda} (2\lambda + 1) j_{\lambda}(Kr) P_{\lambda}(\cos \theta), \quad (9)$$

where θ is the angle between \vec{K} and \vec{r} , P_{λ} is the Legendre polynomial of order λ , and j_{λ} is the spherical Bessel function of order λ . Then using (9), the expression for the form factor for an $nlm \rightarrow \epsilon l' m'$ transition after integrating out the wave functions of the nonparticipating electrons becomes

$$F_{nlm, \epsilon l' m'}(K) = \sum_{\lambda} (i)^{\lambda} (2\lambda + 1) [(2l + 1)(2l' + 1)]^{1/2} \times (-1)^{m'} \begin{pmatrix} l' & \lambda & l \\ 0 & 0 & 0 \end{pmatrix} \begin{pmatrix} l' & \lambda & l \\ -m' & 0 & m \end{pmatrix} R_{nl, \epsilon l'}^{\lambda}(K), \quad (10)$$

where

$$R_{nl, \epsilon l'}^{\lambda}(K) = \int_0^{\infty} P_{nl}(r) j_{\lambda}(Kr) P_{\epsilon l'}(r) dr, \quad (11)$$

$\begin{pmatrix} l' & \lambda & l \\ 0 & 0 & 0 \end{pmatrix}$ and $\begin{pmatrix} l' & \lambda & l \\ -m' & 0 & m \end{pmatrix}$ are Wigner 3- j symbols,²⁰ and the sum over λ goes from $|l' - l|$ to $l' + l$ in steps of two; the 3- j symbol $\begin{pmatrix} l' & \lambda & l \\ 0 & 0 & 0 \end{pmatrix}$ vanishes for all other values of λ . The absolute square of the form factor for an $nl \rightarrow \epsilon l'$ transition from a closed subshell, summed over final degenerate magnetic substates m' and average over initial substates m , is then

$$|F_{nl, \epsilon l'}(K)|^2 = \sum_{\lambda, \lambda'} i^{\lambda - \lambda'} (2\lambda + 1)(2\lambda' + 1) \times (2l' + 1) \begin{pmatrix} l' & \lambda & l \\ 0 & 0 & 0 \end{pmatrix} \begin{pmatrix} l' & \lambda' & l \\ 0 & 0 & 0 \end{pmatrix} R_{nl, \epsilon l'}^{\lambda}(K) R_{nl, \epsilon l'}^{\lambda'}(K) \times \sum_{m, m'} \begin{pmatrix} l' & \lambda & l \\ -m' & 0 & m \end{pmatrix} \begin{pmatrix} l' & \lambda' & l \\ -m' & 0 & m \end{pmatrix}. \quad (12)$$

The sum over m and m' is, owing to the properties of the 3- j symbols, $[1/(2\lambda + 1)] \delta_{\lambda \lambda'}$, so that the absolute square of the form factor becomes

$$|F_{nl, \epsilon l'}(K)|^2 = (2l' + 1) \sum_{\lambda} (2\lambda + 1) \times [R_{nl, \epsilon l'}^{\lambda}(K)]^2 \left| \begin{pmatrix} l' & \lambda & l \\ 0 & 0 & 0 \end{pmatrix} \right|^2 \quad (13)$$

and the cross section becomes

$$\sigma_{nl, \epsilon l'} = \frac{8\pi a_0^2 z^2}{m v^2 / \mathcal{R}} (2l' + 1) \sum_{\lambda} (2\lambda + 1) \left| \begin{pmatrix} l' & \lambda & l \\ 0 & 0 & 0 \end{pmatrix} \right|^2 \times \int_{K_{\min}}^{K_{\max}} \frac{[R_{nl, \epsilon l'}^{\lambda}(K)]^2}{(Ka_0)^2} d \ln(Ka_0)^2. \quad (14)$$

This result shows that the transition probability for unpolarized targets can be expressed as an incoherent sum of contributions for alternative values of angular momentum $\hbar\lambda$ transferred to the target atom by the interaction. This is a particular example of a general feature of collision processes involving unpolarized targets as shown by Fano and Dill.²¹

In the ionized continuum, however, at each energy there is an infinite-fold degeneracy among the states of different angular momentum. The relevant measurable physical cross section is the sum over all final angular momenta l' ,

$$\sigma_{nl, \epsilon} = \sum_{l'=0}^{\infty} \sigma_{nl, \epsilon l'}, \quad (15)$$

with the associated GOS

$$f_{nl, \epsilon}(K) = (\epsilon - \epsilon_{nl}) (Ka_0)^{-2} \sum_{l'=0}^{\infty} |F_{nl, \epsilon l'}(K)|^2 \quad (16)$$

and form factor

$$|F_{nl, \epsilon}(K)|^2 = \sum_{l'=0}^{\infty} |F_{nl, \epsilon l'}(K)|^2. \quad (17)$$

In practice, however, all but the first few terms in the sums [Eqs. (15)–(17)] are negligible for low enough ionized-electron energy ϵ . These calculations consider $l' = 0-8$ and were performed numerically on an IBM 7094. The errors produced by the omission of higher l' terms will be discussed in the Sec. III.

III. RESULTS AND DISCUSSION

Calculations have been performed for the ionization of $2s$ and $2p$ electrons in Al by the methods described in the Sec. II. We have considered ionized electron energies from threshold ($\epsilon = 0$) to $\epsilon = 128$ Ry. Since the cross sections are integrals over the generalized oscillator strengths [Eq. (5)], it is of interest to study the latter quantities first.

A. Generalized Oscillator Strengths (GOS)

The GOS results for $2p$ ionization from threshold to $\epsilon = 8$ Ry is shown in Fig. 1. Here we find a marked departure from the decreasing behavior of the GOS, as a function of ionized-electron energy in rydbergs ϵ/R , which is typical of the hydrogenic results⁵ and of the higher energies (shown in Fig. 2). The GOS increases from threshold to $\epsilon/R = 2$ for all (Ka_0) , and only then does it begin to decrease with energy. In the limit of $K \rightarrow 0$, the GOS approaches the *optical* oscillator strength¹⁸ which, in the ionized continuum, is proportional to the photoionization cross section.⁷ Thus it follows from the results given in Fig. 1 that the Al $2p$ -photoionization cross section will be increasing from threshold to a maximum at about $\epsilon/R = 2$, i. e., it exhibits a *delayed maximum*, a phenomenon which has been observed for various

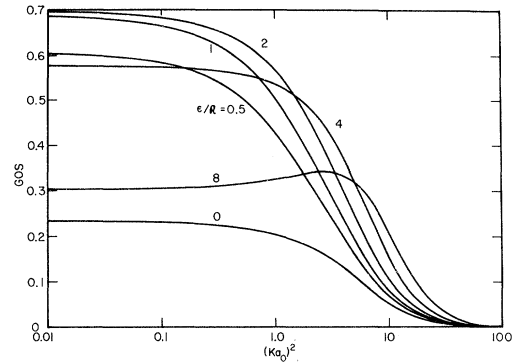


FIG. 1. Generalized oscillator strengths per unit energy in rydbergs for continuum transitions of the $2p$ shell of Al (binding energy 5.947 Ry) for various ionized-electron energies (in rydbergs) ϵ/R .

subshells in many elements.^{7-9,22} This delayed maximum occurs in photoionization, because the $l-l+1$ continuum wave function (the ϵd in this case) is kept very far out at threshold by the repulsive centrifugal barrier causing overlap with the discrete function and, thus, the matrix element, to be quite small. At higher energies, the continuum wave function can penetrate the barrier much more readily, so that its amplitude is larger in the inner region, where the discrete wave function has appreciable amplitude and consequently the photoionization cross section increases. At even higher energies the continuum function moves in still further and the overlap begins to decrease because of cancellation in the matrix element from the oscillations in the continuum wave function, thus causing the decreasing behavior of the photoionization cross section with energy. A much more detailed discussion of the delayed maxima phenomenon in photoionization is given in Ref. 7.

The situation with regard to the GOS is much the same except that the matrix element is of e^{iKz} , rather than z , and there is no $l \pm 1$ selection rule as in the optical case. In Fig. 3 the Al $2p$ GOS's for $\epsilon/R = 0$ and 2 are shown along with the contributions of each individual final continuum angular momentum (l') state. Here we find that the $2p \rightarrow \epsilon s$ and $2p \rightarrow \epsilon p$ contributions to the GOS decrease somewhat with energy, since the $l' = 0$ and $l' = 1$ waves are penetrating even at threshold. The $2p \rightarrow \epsilon d$ contribution, on the other hand, increases sharply with energy for the same reason as in the optical case. This is the same continuum wave function and, since this channel gives the major contribution to the GOS at these energies, the GOS increases with energy from threshold. The higher partial waves have negligible contributions, because their high angular momentum makes the centrifugal barrier insurmountable at low ener-

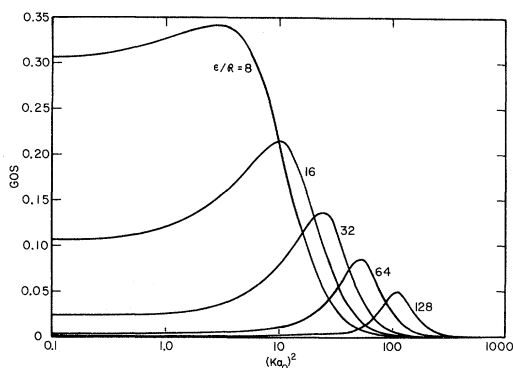


FIG. 2. Generalized oscillator strengths per unit energy in rydbergs for continuum transition of the $2p$ shell of Al (binding energy 5.947 Ry) for various ionized-electron energies (in rydbergs) ϵ/R .

gies. The $l' = 3$ (ϵf) wave, which has essentially no effect at threshold, penetrates far enough to have a very slight effect at $\epsilon/R = 2$ as shown in Fig. 3. Thus we see that the contributions to the GOS of all higher partial waves will increase with energy, until they penetrate sufficiently, and only then start to decrease. The GOS will be decreasing with energy in this region, however, since the major contributors to the GOS are decreasing.

Another point of interest is the difference in shapes between low-energy GOS's as shown in Fig. 1, and those of higher energy which are given in Fig. 2. The GOS at low energy has its maximum at $K = 0$, indicating that the optically allowed (dipole) transitions $2p \rightarrow \epsilon s$ and $2p \rightarrow \epsilon d$ are the dominant partial waves. Physically this means that collisions with small energy transfer take place predominantly with small momentum transfer, i.e., distant large impact parameter collisions. At the higher energies, particularly the highest we have considered, $\epsilon/R = 128$, the maximum is out at a finite value of Ka_0 and moves out with increasing energy. Examination of Fig. 2 shows that, at the maximum point, the relationship between ϵ and K is approaching $\epsilon/R = (Ka_0)^2$. This is just the relationship one would obtain for collisions with a *free* electron. Thus, we have the situation where the collisions are close (knock-on), and the binding of the electron serves simply to smear out the collisions over a small range of momentum transfers. Mathematically, this occurs because at high energy the continuum wave function reaches its asymptotic form $\sin(\epsilon^{1/2}r + \delta)$ at fairly small R , while for large K the spherical Bessel function quickly reaches its asymptotic form of $\sin(Kr + \eta)$, so that for $Ka_0 = (\epsilon/R)^{1/2}$ there is constructive interference and, hence, a maximum. This maximum, plotted on a three-dimensional GOS versus ϵ/R and $(Ka_0)^2$ graph, is known as the Bethe ridge.²

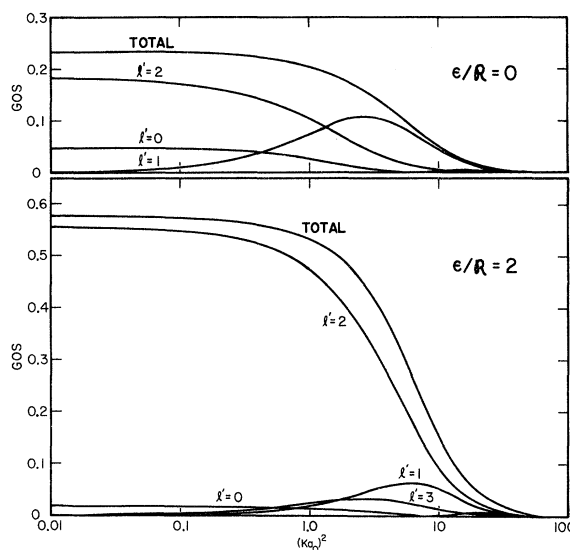


FIG. 3. Contributions to the Al $2p$ GOS by the various continuum angular momentum (l') channels for ionization at threshold and $\epsilon/R = 2$.

The GOS's for Al $2s$ are shown in Figs. 4 and 5 for low and high energy, respectively. Over the entire energy range, the limiting $Ka_0 \rightarrow 0$ value of the GOS is decreasing with increasing ϵ , indicating a monotone decreasing photoionization cross section. There is some anomalous behavior of the GOS at the lower energies at intermediate momentum transfer, where the GOS's from $\epsilon/R = 0.5$ to $\epsilon/R = 8$ have their maxima. The GOS in this region increases with ϵ from threshold to $\epsilon/R = 2$, in contradistinction to the decreasing behavior at small Ka_0 . This can be understood by considerations similar to those previously discussed for the $2p$. The $2s \rightarrow \epsilon d$ is an optically forbidden transition so it does not contribute to the GOS for small Ka_0 ; only the $2s \rightarrow \epsilon p$ channel does, and since the ϵp is penetrating even at threshold, the GOS at the optical limit is monotone decreasing with energy.

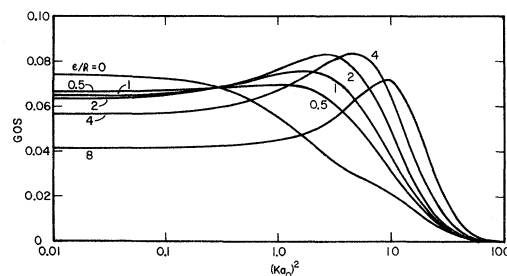


FIG. 4. Generalized oscillator strengths per unit energy in rydbergs for continuum transitions of the $2s$ shell of Al (binding energy 8.715 Ry) for various ionized-electron energies (in rydbergs) ϵ/R .

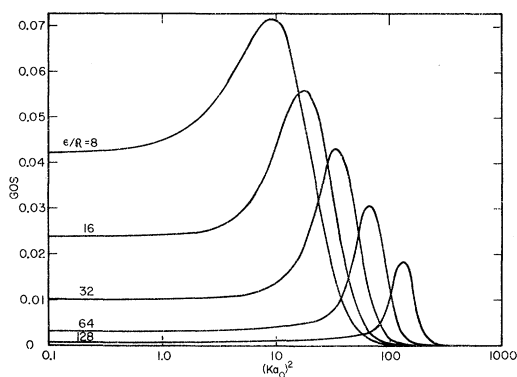


FIG. 5. Generalized oscillator strengths per unit energy in rydbergs for continuum transitions of the $2s$ shell of Al (binding energy 8.715 Ry) for various ionized-electron energies (in rydbergs) ϵ/R .

Away from this limit the $2s \rightarrow \epsilon d$ channel is a significant fraction of the GOS. At threshold it is fairly small, due to the inability of the ϵd continuum function to penetrate very much at $\epsilon/R=0$, but even here shows up as a bump on the tail of the threshold GOS at $(Ka_0)^2 \approx 10$. At slightly higher energies (up to $\epsilon/R \approx 2$) the ϵd penetrates more and more, making the $2s \rightarrow \epsilon d$ the dominant contribution and, thus, steadily increasing the GOS with energy. At still higher energies, further penetration of the ϵd causes a decrease in overlap, due to its oscillations, thus decreasing the GOS, just as in the $2p$ case. At the higher energies (shown in Fig. 5), everything is quite normal, and we see again here the manifestation of the Bethe ridge for $\epsilon/R \approx (Ka_0)^2$.

The total GOS results presented herein are sums over the partial wave channels $l'=0$ to 8; those with $l' \geq 9$ have been neglected in the sum indicated by Eq. (14). To investigate the effect of the omitted terms, consider the $l'=9$ continuum wave channel. In our calculation a continuum wave sees an effective central potential $V(r) + l'(l'+1)/r^2$ [c.f. Eq. (6)] which is $V(r) + 90/r^2$ for $l'=9$. Since most of the amplitude of the $2s$ and $2p$ orbitals of Al is at a distance $r \gtrsim 1$ (in units of a_0) from the nucleus, a continuum wave function must penetrate appreciably at least this far in to have enough overlap with the discrete functions to give a non-negligible contribution to the total GOS. The effective potential of Al at $r=1$ is dominated by the centrifugal repulsion term for an l' of 9; the sum of the two terms is about 85 Ry. Thus the omission of the $l'=9$ partial wave will have virtually no effect at ejected electron energies much below this energy. It will, therefore, affect somewhat our $\epsilon/R=128$ GOS results but not the lower-energy ones. In fact the $\epsilon/R=128$ GOS will not be greatly altered since even this high an energy continuum

wave will not penetrate in closer than the outer edge of the discrete functions. By the above arguments then, $l' > 9$ channels will be still less important. Therefore we conclude that the omitted channels will not affect any of the lower energies ($\epsilon/R \leq 64$) and will add only $< 5\%$ to the GOS at $\epsilon/R = 128$.

B. Cross Sections

Once a knowledge of the GOS is obtained, the cross section for the inelastic scattering of any fast (structureless) charged particle can be found by the integration indicated by Eq. (5). It must be emphasized, however that the GOS is an intrinsic function of the atom itself, much like the optical oscillator strength, and *not* dependent upon the incident particle, and the details of the interaction are implicitly contained in the K dependence.

We have considered L -shell ionization by protons with incoming energies of 0.1, 1, 10, and 100 MeV. The calculated cross sections for producing electrons with a particular energy from the $2p$ subshell, i.e., the energy-loss cross sections, are shown in Fig. 6. The outstanding feature of these results is the behavior of the cross sections at small energy loss, near the ionization threshold; they *increase* from threshold with increasing energy loss reaching maxima at ϵ/R between 0.5 and 1, and only then do they decrease with increasing ϵ . This is in marked contradistinction

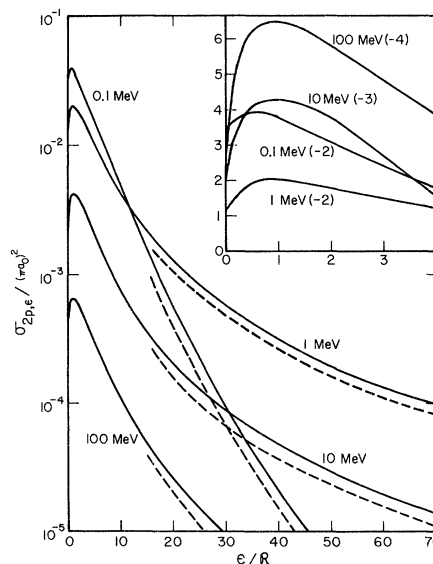


FIG. 6. Energy-loss cross sections in the continuum for 0.1-, 1-, 10-, and 100-MeV protons incident on the $2p$ shell of Al vs ionized-electron energy in rydbergs. The insert shows the threshold region in detail with the number in parentheses for each curve being the power of 10 the scale must be multiplied by. The dashed curves are the hydrogenic results.

to the previous hydrogenic results which decrease monotonically from threshold.¹⁰ These *delayed maxima* in the energy-loss cross sections are a direct consequence of the same phenomena in the GOS discussed in Sec. II. Since the cross sections are integrals over the GOS's divided by the energy loss, they exhibit this phenomenon for precisely the same reasons the GOS's do; the centrifugal barrier keeping the higher-angular-momentum continuum waves far out at threshold. It is also seen from the insert in Fig. 6 that the delayed maximum moves further out to greater ϵ and the rise in cross section from threshold to maximum increases (percentagewise) with increasing proton energy. To explain this, we first note that the lower limit on the momentum transfer in the integral performed to obtain the cross section [Eq. (5)] can be well approximated by¹⁸

$$(Ka_0)_{\min}^2 = (M/m) (\Delta E^2/4TR), \quad (18)$$

if the incident energy $T \gg \Delta E$, the energy loss; the upper limit, under these conditions, can be taken to be $(Ka_0)_{\max}^2 = \infty$ to an excellent approximation.¹⁸ Thus, apart from an over-all factor of $1/T$, the only effect of increasing the incident energy is to *decrease* $(Ka_0)_{\min}$, thereby including in the integral more of the GOS near the optical limit. Since, in this region $f_{2p,\epsilon}(K)/\Delta E$ has a maximum at about $\epsilon/R=1$, a result easily obtained from Fig. 1, the maximum of the integral, and thus the energy-loss cross section, will move toward this energy with increasing T . At small T , however, where the integral samples the intermediate and large $(Ka_0)^2$ regions of the GOS, where it is quite regular, the energy-loss cross section decreases from threshold. Thus the maximum must move out to greater energy loss with increasing T , as we have found. Further, since the ratio of the GOS's for $\epsilon/R=1$ and 0 is greatest at the optical limit, as seen from Fig. 1, the effect of increasing T and including in the integral more of the GOS near the optical limit is to *increase* the ratio of the cross sections at these energies, i. e., the rise in the cross section from threshold to the maximum will increase (percentagewise) with increasing T .

Rather than considering the total energy-loss cross section as an *integral over the sum* of the GOS's of each of the continuum angular momentum channels, it can be thought of as a *sum over the integrals* of each channel as given by Eq. (14). In an effort to provide further insight into the behavior of the cross section, Fig. 7 shows the total energy-loss cross section $\sigma_{2p,\epsilon}$ along with the contributions of each partial wave $\sigma_{2p,\epsilon l'}$ for $T=10$ MeV. The $l'=0$ and 1 contributions decrease monotonically from threshold indicating that the centrifugal barrier is absent ($l'=0$) or is too small to repel the continuum wave at threshold ($l'=1$).

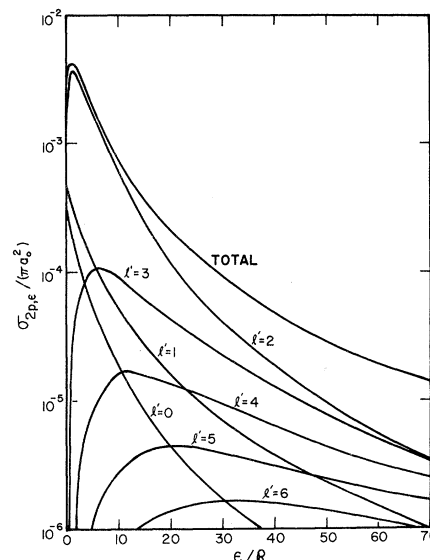


FIG. 7. Continuum energy-loss cross section for 10-MeV protons incident on the $2p$ shell of Al vs ionized-electron energy in rydbergs along with the contributions of each final angular momentum (l') channel.

For $l' \geq 2$, the barrier gets larger and larger with increasing l' , resulting in a maximum for $l'=2$ just above threshold, somewhat further out for $l'=3$ and moving out still further for higher partial waves. Since the dominant term is the $l'=2$, the total tends to have its character, giving rise to the curve shown in Fig. 7.

The calculated energy-loss cross sections for ionization of $2s$ electrons are given in Fig. 8. These results also show the delayed maximum, just as the $2p$ did, but with two important differences. First, the maximum is at about $\epsilon/R=0.75$ for proton energies of 0.1 and 1 MeV and moves in to lower ϵ for greater T . Second, the (percentage) rise in the cross section from threshold to maximum *decreases* from $T=0.1$ to 100 MeV, where it is almost flat. This behavior can be understood by considering the GOS results for the $2s$ subshell shown in Fig. 4. Here, as was noted in Sec. II, the GOS results show the normal monotone decrease, with increasing energy loss, for small momentum transfer [$(Ka_0)^2 \sim 0.01$] but anomalies appear at intermediate values [$(Ka_0)^2 \sim 1$]. Thus, for $T=0.1$ MeV, the important region of the integral [Eq. (5)] is the intermediate values of momentum transfer which gives a delayed maximum. At higher values of T , the integral includes more of the small $(Ka_0)^2$ contribution, since K_{\min} decreases, and this contribution is decreasing with increasing ϵ . Hence, the net effect of increasing T must be to move the delayed maximum in towards threshold and decrease its value relative to threshold value of the cross section.

Clearly then, for $T > 100$ MeV, the cross section will be *decreasing* from threshold, based on the above arguments. We shall discuss this point further in the Sec. IV.

Apart from our calculations using HS wave functions, we have also performed numerical hydrogenic calculations for purposes of comparison and checking. We have used the Slater inner screening constant²³ of 4.15 which is appropriate to a filled L shell, (effective Z is $Z - 4.15$), and outer screening¹⁰ parameters to reproduce the HS $2s$ and $2p$ binding energies. Energies $\epsilon/R \geq 16$ have been considered; we have omitted small ϵ/R , because this necessitated extrapolation into the hydrogenic discrete range. This, however, is being studied by Basbas.²⁴

The results of these hydrogenic calculations for the $2p$ and $2s$ subshells of Al are shown as dashed curves in Figs. 6 and 8, respectively, where it is seen that agreement between the hydrogenic and HS results is fairly good (no worse than 30%) for both subshells at intermediate *and* high-energy loss. This is expected for intermediate values of ϵ , since the major contribution to the matrix element [Eq. (11)] here comes from intermediate distances from the nucleus, where the hydrogenic wave functions are a good approximation. At the higher energy losses one is tempted to say that the largest contribution to the matrix element comes from close in by the nucleus be-

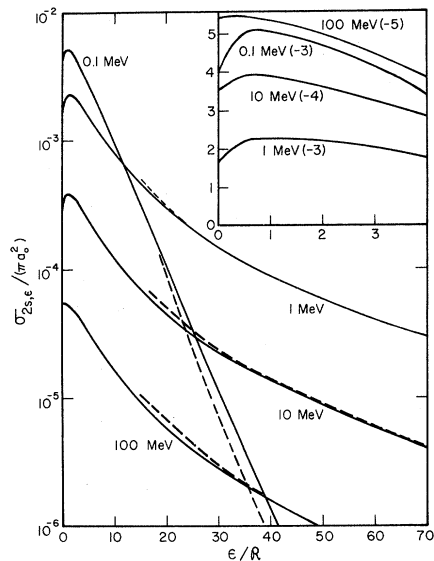


FIG. 8. Energy-loss cross sections in the continuum for 0.1-, 1-, 10-, and 100-MeV protons incident on the $2s$ shell of Al vs ionized-electron energy in rydbergs. The insert shows the threshold region in detail with the number in parentheses for each curve being the power of 10 the scale must be multiplied by. The dashed curves are the hydrogenic results.

cause of the oscillations of the continuum wave functions, as in the case of photoionization. This argument is abnegated by the fact that the spherical Bessel function $j_\lambda(Kr)$ appears in the matrix element. This is another oscillatory function whose oscillations are not small compared to the continuum functions. As discussed previously, the maximum in the GOS for large ϵ is at the Bethe ridge $(Ka_0)^2 = \epsilon/R$, where the continuum wave functions and $j_\lambda(Kr)$ interfere constructively, so that the major part of the matrix element is generated at intermediate, not small, distances from the nucleus.

To illustrate the situation in the threshold region we have computed the total L -shell energy-loss cross section from the analytic formula for the L -shell form factor^{10,11} and compared with the sum of our HS $2s$ and $2p$ results, shown in Fig. 9. The hydrogenic result is seen to vastly overestimate the cross section at threshold by about a factor of 5. Further, it is monotone decreasing from threshold, while the HS results show the delayed maximum. This poor agreement has several important implications. First, the hydrogenic total ionization cross section, which is the area under the energy-loss cross-section curve, will be much too large compared to the HS because of its tremendous maximum in the threshold region where most of the area comes from. Second, the same will be true for the stopping power. Finally, the contribution to the stopping power from excitations to discrete states, which is often obtained by extrapolation of the ionization cross section, will be grossly overestimated by the hydrogenic results, by roughly an order of magnitude. In view of these limitations of the hydrogenic approximation, it seems necessary to calculate the shell correction to the stopping power for the Al L shell using our more realistic wave functions, which has been done to date using only hydrogenic functions.¹¹ This is especially desirable in view of the fact that stopping-power measurements can be made with an accuracy of $\sim 0.1\%$.

A further comparison of interest is between the hydrogenic and HS calculations of the contributions of each of the continuum angular-momentum channels. While measurements of the energy-loss cross section looks at only the total, the sum over all channels, the relative contributions of the individual channels, are important for calculations of the angular distribution of ionized electrons and the angular correlation between scattered particles and ionized electrons, experiments on which have been done only recently.²⁵⁻²⁷ In Table I, the comparison for Al $2p$, $T = 10$ MeV, $\epsilon/R = 16$ and 128 is given and shows that, in both cases, while the totals, the sum of the individual channels, are fairly close, the individual channels are often very

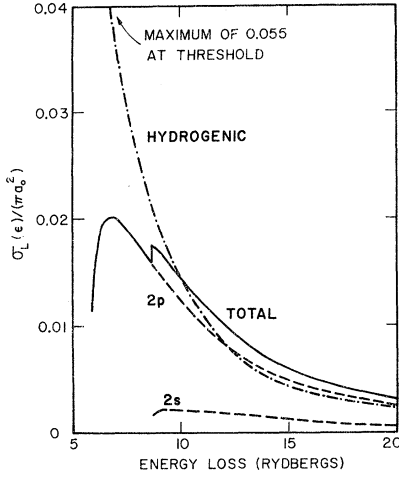


FIG. 9. Total L -shell continuum energy-loss cross section for 1-MeV protons. The solid curve is our present result, the dashed curves are the contributions of the individual subshells, and the dot-dashed curve is the hydrogenic result.

different. This indicates that although the total energy-loss cross section predicated by the hydrogenic model may be fairly good, the angular distributions or correlations may be seriously in error.

It has recently been pointed out²⁸ that somewhat more realistic results can be obtained in the hydrogenic formulation, by using a Coulomb $z = 1$ continuum wave function orthogonalized to the initial (nl) state of the ionized electron. This formulation has the advantage of still being analytic and having the correct asymptotic charge at infinity. Further, the orthogonalization essentially introduces a reasonable phase shift into the $nl \rightarrow \epsilon l$ channel. Unfortunately, the $l \rightarrow l+1$ and $l \rightarrow l+2$ channels, which are dominant near threshold, are unaltered in this formulation and although this represents a slight improvement over ordinary hydrogenic, it is still quite deficient since, as shown above, phase shift and normalization variations near threshold in the

ϵd channel are crucial and these are neglected in this model. Another recent calculation²⁸ has used this model but with analytic Hartree-Fock initial states. In a previous paper,³⁶ we have compared our results and these for the continuum GOS of argon and found almost an order of magnitude difference near threshold. Thus we conclude that the above orthogonalization does not significantly improve the results near threshold.²⁹

C. Bethe Asymptotic Cross Sections

For large incident energy T , the energy-loss cross section approaches a particularly simple form. Specifically, if we define the *reduced* incident energy of an incoming particle of mass M to be $\bar{T} = (m/M)T$, m being the electron mass, the cross section approaches its asymptotic behavior when $\Delta E/\bar{T} \ll 1$, i. e., when the energy loss is much smaller than the reduced incident energy. In this limit the energy-loss cross section to a particular final angular momentum channel is^{3,18}

$$\sigma_{nl, \epsilon l'} = \frac{4\pi a_0^2 z^2}{\bar{T}/R} \left[M_{nl}^{l'}(\epsilon)^2 \ln \left(\frac{4c_{nl}^{l'}(\epsilon)\bar{T}}{R} \right) + O \left(\frac{1}{\bar{T}/R} \right) \right] \quad (19)$$

for an optically accessible final state, and

$$\sigma_{nl, \epsilon l'} = \frac{4\pi a_0^2 z^2}{\bar{T}/R} \left[b_{nl}^{l'}(\epsilon) + O \left(\frac{1}{\bar{T}/R} \right) \right] \quad (20)$$

for a transition to an optically forbidden final state. In these relations $M_{nl}^{l'}(\epsilon)$ is the dipole matrix element $\langle nl | z | \epsilon l' \rangle$ and the parameters $c_{nl}^{l'}(\epsilon)$ and $b_{nl}^{l'}(\epsilon)$ are given by^{3,18}

$$\ln \left[c_{nl}^{l'}(\epsilon) \left(\frac{\Delta E}{R} \right)^2 \right] = \int_0^\infty \frac{f_{nl, \epsilon l'}(K)}{f_{nl, \epsilon l'}} d \ln(Ka_0)^2 - \int_{-\infty}^0 \left(1 - \frac{f_{nl, \epsilon l'}(K)}{f_{nl, \epsilon l'}} \right) d \ln(Ka_0)^2, \quad (21)$$

$$b_{nl}^{l'}(\epsilon) = \int_{-\infty}^\infty \frac{f_{nl, \epsilon l'}(K)}{\Delta E/R} d \ln(Ka_0)^2, \quad (22)$$

TABLE I. Contributions to the energy-loss cross section of each continuum angular momentum (l') channel for 10-keV protons on the $2p$ subshell of Al and $\epsilon/R = 16$ and 128. The result of the HS calculation, numerical hydrogenic (H) result, and their ratio is shown in each case. In this table read 3.21-4 as 3.21×10^{-4} .

ϵ/R		Total	$l'=0$	1	2	3	4	5	6	7	8
16	HS	3.21-4	7.04-6	2.43-5	2.09-4	5.91-5	1.53-5	4.17-6	1.21-6	3.57-7	1.07-7
	H	2.58-4	5.80-6	1.03-5	2.02-4	1.37-5	1.37-5	1.68-6	1.56-7	1.18-8	7.58-10
	HS/H	1.24	1.21	2.36	1.03	2.38	1.12	2.48	7.75	30.2	141
128	HS	3.52-6	4.76-8	1.91-7	5.35-7	6.85-7	6.42-7	5.25-7	4.01-7	2.91-7	2.05-7
	H	3.04-6	4.92-8	6.67-8	4.78-7	2.18-7	6.67-7	5.77-7	4.47-7	3.21-7	2.18-7
	HS/H	1.16	0.97	2.86	1.12	3.14	0.96	0.93	0.90	0.91	0.92

with $f_{nl, \epsilon l'}$, the optical oscillator strength for a $nl \rightarrow \epsilon l'$ transition [$= f_{nl, \epsilon l'}(0)$].

The importance of the parametrization is two-fold. First, it offers a convenient way of characterizing the cross section for $\Delta E/\bar{T} \ll 1$ (which is just the region where first Born approximation is expected to be valid), so that these parameters contain essentially all of the meaningful content of the Born approximation. Second, and more important, using these parameters we can extend our results into the relativistic region ($\bar{T} \gtrsim mc^2$), even though they were obtained from an explicitly non-relativistic calculation. For relativistic incident particles with velocity $v = \beta c$, c being the velocity of light, Eqs. (18) and (19) must be modified.^{1,30,31} The result is³

$$\sigma_{nl, \epsilon l'} = \frac{8\pi\alpha_0^2 z^2}{mv^2/\mathcal{R}} \left\{ M_{nl}^{l'}(\epsilon)^2 \left[\ln\left(\frac{\beta^2}{1-\beta^2}\right) - \beta^2 \right] + C_{nl}^{l'}(\epsilon) \right\} \quad (23)$$

for allowed transitions, and

$$\sigma_{nl, \epsilon l'} = \frac{8\pi\alpha_0^2 z^2}{mv^2/\mathcal{R}} b_{nl}^{l'}(\epsilon) \quad (24)$$

for optically forbidden transitions. The new parameter in Eq. (23) is related to $c_{nl}^{l'}(\epsilon)$ by^{32,33}

$$\begin{aligned} C_{nl}^{l'}(\epsilon) &= M_{nl}^{l'}(\epsilon)^2 [\ln c_{nl}^{l'}(\epsilon) + \ln(2mc^2/\mathcal{R})], \\ \ln(2mc^2/\mathcal{R}) &= 11.2268. \end{aligned} \quad (25)$$

The Bethe asymptotic parametrization of the total energy-loss cross section, $\sigma_{nl, \epsilon}$ can be obtained simply by summing over the asymptotic cross sections to each final angular-momentum channel, Eqs. (19) and (20) [Eqs. (23) and (24) in the relativistic case]. If we define for *optically allowed* channels

$$b_{nl}^{l'}(\epsilon) = M_{nl}^{l'}(\epsilon)^2 \ln c_{nl}^{l'}(\epsilon), \quad (26)$$

we then get

$$\begin{aligned} \sigma_{nl, \epsilon} &= \frac{4\pi\alpha_0^2 z^2}{\bar{T}/\mathcal{R}} \left[M_{nl}^{\text{TOT}}(\epsilon)^2 \ln\left(\frac{4\bar{T}}{\mathcal{R}}\right) \right. \\ &\quad \left. + b_{nl}^{\text{TOT}}(\epsilon) + O\left(\frac{1}{\bar{T}/\mathcal{R}}\right) \right], \end{aligned} \quad (27)$$

with

$$M_{nl}^{\text{TOT}}(\epsilon)^2 = M_{nl}^{l=1}(\epsilon)^2 + M_{nl}^{l=2}(\epsilon)^2 \quad (28)$$

and

$$b_{nl}^{\text{TOT}}(\epsilon) = \sum_{l'=0}^{\infty} b_{nl}^{l'}(\epsilon), \quad (29)$$

which can be written, using Eqs. (21), (22), and (25), as

$$b_{nl}^{\text{TOT}}(\epsilon) = \int_0^{\infty} \frac{f_{nl, \epsilon}(K)}{\Delta E/\mathcal{R}} d \ln(Ka_0)^2$$

$$- \int_{-\infty}^0 \frac{f_{nl, \epsilon}(0) - f_{nl, \epsilon}(K)}{\Delta E/\mathcal{R}} d \ln(Ka_0)^2 \quad (30a)$$

$$\begin{aligned} &= M_{nl}^{\text{TOT}}(\epsilon)^2 \left[\int_0^{\infty} \frac{f_{nl, \epsilon}(K)}{f_{nl, \epsilon}(0)} d \ln(Ka_0)^2 \right. \\ &\quad \left. - \int_{-\infty}^0 \left(1 - \frac{f_{nl, \epsilon}(K)}{f_{nl, \epsilon}(0)} \right) d \ln(Ka_0)^2 \right], \end{aligned} \quad (30b)$$

with $f_{nl, \epsilon}(0) = (\Delta E/\mathcal{R}) M_{nl}^{\text{TOT}}(\epsilon)^2$, the total optical oscillator strength. Thus the total energy-loss cross section and its variation with energy loss can be characterized by $M_{nl}^{\text{TOT}}(\epsilon)$ and $b_{nl}^{\text{TOT}}(\epsilon)$. It is thus of interest to investigate the behavior of these quantities. It is of particular importance because, although the detailed variation of $M_{nl}^{\text{TOT}}(\epsilon)$ is known throughout the periodic system through photoionization and photoexcitation work,²² $b_{nl}^{\text{TOT}}(\epsilon)$ has been looked at only for atomic hydrogen and helium.² We shall therefore study this latter quantity for continuum transitions from the aluminum L shell in an effort to understand the details of its behavior.

Before looking at our numerical results, however, it is of interest to note the information that can be obtained directly from the analytical expressions for the parameters. For optically forbidden transitions, $b_{nl}^{l'}(\epsilon)$ is the *total* area under the $f_{nl, \epsilon l'}(K)/\Delta E$ -vs- $\ln(Ka_0)^2$ curve, as seen from Eq. (22); it is therefore a positive definite quantity, and the contribution of each optically forbidden channel to $b_{nl}^{\text{TOT}}(\epsilon)$ is then positive. The $b_{nl}^{l'}(\epsilon)$ for optically accessible final states, on the other hand, can be positive *or* negative as seen from Eqs. (21) and (23). The parameter $c_{nl}^{l'}(\epsilon)$, discussed in detail by Miller and Platzman,¹⁸ depends only on the *shape* of $f_{nl, \epsilon l'}(K)$ and not upon its magnitude.

Our results for the $2p$ subshell $b_{2p}^{\text{TOT}}(\epsilon)$ are shown in Fig. 10 for small energy loss, along with the individual channel $b_{2p}^{l'}(\epsilon)$ results, whose sum is $b_{2p}^{\text{TOT}}(\epsilon)$. From Fig. 11 it is seen that $b_{2p}^{\text{TOT}}(\epsilon)$ is negative at threshold and decreases to a minimum (maximum in absolute value) at $\epsilon/\mathcal{R} \approx 1$; then increases toward zero with increasing ϵ/\mathcal{R} . The results for higher energy losses are shown in Fig. 11, where we find that $b_{2p}^{\text{TOT}}(\epsilon)$ increases through zero at $\epsilon/\mathcal{R} \approx 19$, and a maximum is reached at $\epsilon/\mathcal{R} \approx 33$ followed by monotonically decreasing behavior with increasing ϵ/\mathcal{R} . The dependence of $b_{2p}^{\text{TOT}}(\epsilon)$ on ϵ thus has two turning points, a minimum near threshold and a maximum at intermediate energy loss, quite markedly different from the hydrogenic results.^{2,34} At the lower energy losses the main contribution, as seen from Fig. 11, is from the $l'=2$ final channel. Here, the negativeness of

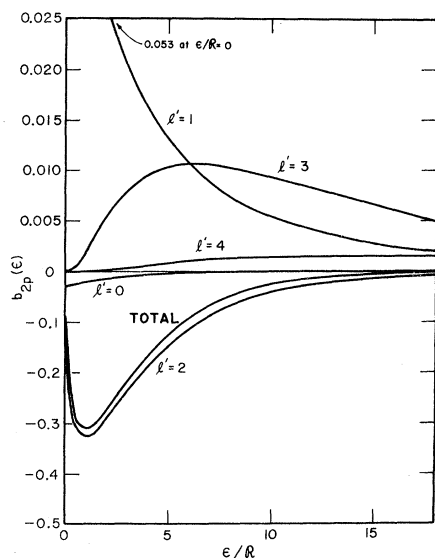


FIG. 10. Dependence of the $b_{2p}^{\text{TOT}}(\epsilon)$ parameter of the Bethe cross section on ionized-electron energy in rydbergs ϵ/R , along with the $b_{2p}^{l'}(\epsilon)$, the contributions of the individual final angular momentum (l') channels. Note the differing scales above and below the axis.

$$b_{2p}^d(\epsilon) = M_{2p}^d(\epsilon)^2 \ln c_{2p}^d(\epsilon)$$

is a consequence of the fact that $\ln c_{2p}^d(\epsilon)$ is negative due to the shape of $f_{2p,ed}(K)$ for small energy loss as previously discussed, while the minimum (maximum in absolute value) at $\epsilon/R \approx 1$ is caused by the delayed maximum in $M_{2p}^d(\epsilon)$, a phenomenon with many other implications as we have already seen. At the higher energy losses (Fig. 11) the optically allowed channels are seen to become less important. The maximum in $b_{2p}^{\text{TOT}}(\epsilon)$ is a consequence of the balance between the increasing optically allowed contributions and decreasing optically forbidden. The higher-angular-momentum final states make almost no contribution at small energy loss because of centrifugal repulsion but become increasingly important at the larger energy losses, as seen in the insert in Fig. 11, where they can penetrate the atomic L shell appreciably.

The results for the $2s$ subshell are shown in Figs. 12 and 13 for small and large energy loss, respectively. The situation here is quite a bit like the $2p$ with one major difference; the minimum value of the allowed channel contribution (and thus the total) is at threshold. This is due to the fact that the dipole matrix element $M_{2s}^p(\epsilon)$ has no delayed maximum in this case. As seen previously, it decreases from threshold leading to the behavior of $b_{2s}^{\text{TOT}}(\epsilon)$ shown in Fig. 12. The maximum in $b_{2s}^{\text{TOT}}(\epsilon)$ and the higher-energy-loss behavior is substantially the same as the $2p$ case and thus require no further discussion.

It can be shown on general grounds that asymptotically³⁵

$$b_{nl}^{\text{TOT}}(\epsilon) = N_{nl} [(\Delta E/R)^{-3}],$$

with N_{nl} the number of electrons in the nl subshell. This asymptotic form is shown as a dashed curve in Fig. 11 and 13 for $2p$ and $2s$, respectively. These plots show that $b_{2p}^{\text{TOT}}(\epsilon)$ effectively reaches its asymptotic form at $\epsilon/R \approx 50$ or about 8 threshold units; $b_{2s}^{\text{TOT}}(\epsilon)$, on the other hand, is still only about 60% of the asymptotic value at the highest energy shown. If the onset of the asymptotic region occurs for both the $2s$ and $2p$ subshells at about the same number of threshold energy units of each, the $2s$ would begin further out in energy owing to its greater binding energy. The difference in binding energies, however, is not sufficient to explain the great differences in asymptotic onset between $2s$ and $2p$, although this effect is in the right direction. We thus do not have a clear understanding of the reason for the asymptotic region for $b_{2p}^{\text{TOT}}(\epsilon)$; more experience from further calculation and/or experiment will have to be gained to provide a definitive answer. Once we can predict *a priori*, where the asymptotic region begins, a considerable simplification in the calculation results. To obtain the Bethe cross section one need only do the full calculation up to the point where $b_{nl}^{\text{TOT}}(\epsilon)$ becomes asymptotic. At greater energy loss, only the very much simpler dipole matrix element would then have to be calculated, as seen from Eq. (24). This saving is more than just a calculational convenience, since the number of channels that must be included in the full calculation increases with increasing ionized-electron energy. As ϵ gets very large, the number of channels increases to such a degree that computer-time considerations preclude carrying out calcula-

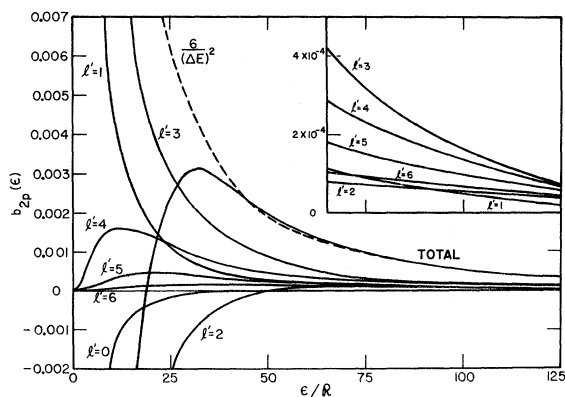


FIG. 11. Dependence of the $b_{2p}^{\text{TOT}}(\epsilon)$ parameter of the Bethe cross section on the ionized-electron energy in rydbergs ϵ/R , along with the individual channel contribution $b_{2p}^{l'}(\epsilon)$. The insert gives some detail at the higher energies and the dashed curve is the asymptotic behavior.

tions. Thus, the fact that we need only do a photoionization calculation at these large energies means that we can extend the Bethe energy-loss cross section to arbitrarily high energy loss without difficulty.

Finally, it is worthwhile to note that the parametrization of the Bethe asymptotic cross section is independent of the mass of the incoming particle, i. e., in the high-energy limit, the cross section is the same for *all* incident particles of the same \bar{T} regardless of their mass. It is only in the next term, the coefficient of $(\bar{T}/R)^{-1}$, that the mass of the incident particle shows up.³²

IV. ACCURACY OF CALCULATED RESULTS

Up to this point no mention has been made of the accuracy of our results. This is of particular importance inasmuch as there is no experimental data on the GOS or energy-loss cross sections of the aluminum *L* shell. Recent GOS calculations³⁶ using precisely the same atomic model employed in this paper have indicated that the GOS results of this paper should be accurate to at least 20% at threshold down to within 10% well above threshold. These same maximum limits of error apply to our energy-loss cross sections provided, of course, that the incident energy is sufficient for the Born approximation to be valid. Based on these estimates of accuracy then, it is expected that the delayed maxima in the energy-loss cross sections are not merely an artifact of this type of calculation, but are real and will be detectable experimentally. In fact, experimental evidence of delayed maxima in the electron energy-loss cross

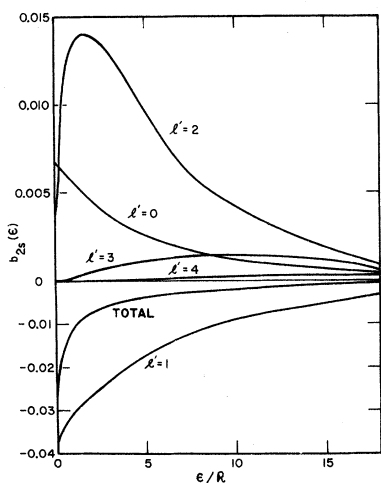


FIG. 12. Dependence of the $b_{2s}^{TOT}(\epsilon)$ parameter of the Bethe cross section on ionized-electron energy in rydbergs ϵ/R , along with the $b_{2s}^{l'}(\epsilon)$, the contributions of the individual final angular momentum (l') channels. Note the differing scales above and below the axis.

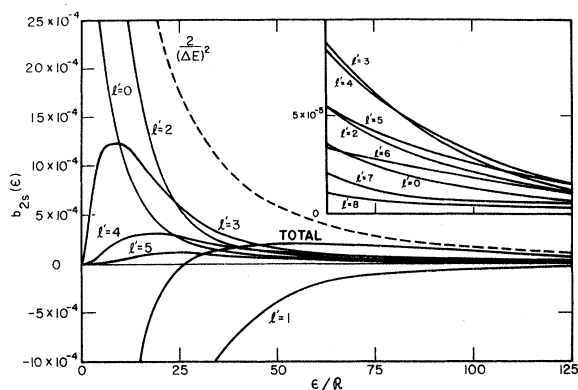


FIG. 13. Dependence of the $b_{2s}^{TOT}(\epsilon)$ parameter of the Bethe cross section on the ionized-electron energy in rydbergs ϵ/R , along with the individual channel contributions $b_{2s}^{l'}(\epsilon)$. The insert gives some detail at the higher energies and the dashed curve is the asymptotic behavior.

sections of the noble gases has been found by Afrosimov *et al.*³⁷ For the $2p$ subshell of Ar the maximum was found to be about 6 eV above threshold for incoming 4-keV electrons (which have the same velocity of protons of about 7 MeV). Thus we have qualitative experimental confirmation of our present results, which tends to give one more confidence in their accuracy.

V. CONCLUSIONS

We have presented a fairly accurate calculation of the GOS and energy-loss cross section of the *L* shell of aluminum pointing up the phenomenon of the delayed maxima which has, as has been discussed, a number of important implications for total ionization cross section and stopping power calculations. Another important result was that although the hydrogenic results were quite poor near threshold (almost an order of magnitude too large) by about 50 eV above threshold, they were in very good agreement with our HS calculations. Thus we really needed to do our calculation for only the first 50 eV above threshold for the Al *L* shell. While it seems clear that the hydrogenic results will be good for intermediate and large energy loss for the *L* shells of other elements as well, further experience is necessary to learn at what energy this takes place. To study this, as well as to obtain more information on the details of the delayed maxima, calculations are in progress on the *L* shells of Ne, Si, Ar, and Cu. Preliminary results will be furnished, prior to publication, to anyone requesting them.

The delayed maximum, as we have discussed, is due to the centrifugal barrier keeping the higher-angular-momentum continuum waves far out at threshold. Thus outer shells will also exhibit the delayed-maximum phenomenon. For outer-shell *s* and *p* electrons the delayed maxima will be pretty

much like the L shell, but for d and f electrons it will often be very much sharper and further out in energy, since f and g waves, respectively, are the important continuum channels in these latter cases, and these may reach maxima at much higher energy than the d -wave channel which causes the delayed maxima in the L shell. This has been indicated by the calculations of differential inelastic electron scattering from noble gases by Amusia, Cherepkov, and Sheftel³⁸ and the experimental work of Afrosimov and co-workers.³⁷ It is therefore expected that delayed maxima in energy-loss cross sections, like their counterparts in photoionization, will be a very widespread phenomenon. Further, if it occurs far out in energy, rather than right near threshold as in the case of the L shell, the hydrogenic calculation will be poor in a much larger energy range than in the L -shell

case. Thus results based on the hydrogenic model for d and f shells must be approached with caution. In any case it is clear that a great deal of work, both theoretical and experimental, needs to be done to fully understand the situation.

ACKNOWLEDGMENTS

It is a pleasure to acknowledge the help of Professor U. Fano who suggested this problem and who, along with Dr. Y.-K. Kim and Dr. M. Inokuti, contributed valuable advice and suggestions throughout the course of this work. We are also indebted to Dr. R. Huebner and Dr. D. Dill, along with Dr. Kim, for critically reading the manuscript. Finally, we are grateful to the Georgia State University Computer Center for an extremely generous grant of computer time without which this work could not have been performed.

¹H. Bethe, Ann. Physik 5, 325 (1930); H. Bethe in *Handbuch der Physik*, edited by H. Geiger and K. Scheel (Springer, Berlin, 1933), Vol. 24/1, p. 273.

²M. Inokuti, Rev. Mod. Phys. 43, 297 (1971).

³M. Inokuti, Y.-K. Kim, and R. L. Platzman, Phys. Rev. 164, 55 (1967).

⁴See, for example, the reviews by B. Moiseiwitch and S. Smith, Rev. Mod. Phys. 40, 238 (1968); M. Rudge, *ibid.* 40, 564 (1968); and R. Peterkop and V. Veldre, in *Advances in Atomic and Molecular Physics*, edited by D. R. Bates and I. Estermann (Academic, New York, 1968), Vol. 2, p. 263, and references therein.

⁵H. Hall, Rev. Mod. Phys. 8, 358 (1936).

⁶We use the "Hartree-Slater" terminology to indicate that we have Hartree wave functions with the Slater approximation to exchange; the more usual "Hartree-Fock-Slater" terminology incorrectly suggests an *improvement* on the Fock exchange. We thank Y.-K. Kim for suggesting this change.

⁷S. T. Manson and J. W. Cooper, Phys. Rev. 165, 128 (1968).

⁸E. J. McGuire, Phys. Rev. 175, 20 (1968).

⁹F. Combet-Farnoux, J. Phys. (Paris) 30, 521 (1969).

¹⁰E. Merzbacher and H. W. Lewis in *Handbuch der Physik*, edited by S. Flügge (Springer-Verlag, Berlin, 1958), p. 166.

¹¹M. C. Walske, Phys. Rev. 101, 940 (1956).

¹²E. A. Uehling, Ann. Rev. Nucl. Sci. 4, 315 (1954).

¹³U. Fano, Ann. Rev. Nucl. Sci. 13, 1 (1963).

¹⁴U. Fano and J. E. Turner, in *Studies in Penetration of Charged Particles in Matter*, Natl. Acad. Sci.-Natl. Res. Council Publ. No. 1133 (U.S. GPO, Washington, D.C., 1964), p. 49.

¹⁵H. Bichsel, University of Southern California Report No. 3, 1961 (unpublished).

¹⁶E. J. McGuire, Phys. Rev. A 3, 267 (1971).

¹⁷M. S. Livingston and H. A. Bethe, Rev. Mod. Phys. 9, 282 (1937).

¹⁸W. Miller and R. Platzman, Proc. Phys. Soc. (London) A70, 299 (1957).

¹⁹F. Herman and S. Skillman, *Atomic Structure Calculations* (Prentice-Hall, Englewood Cliffs, N. J., 1963).

²⁰A. Messiah, *Quantum Mechanics* (North-Holland, Amsterdam, 1966), Vol. 2, p. 1054.

²¹U. Fano and D. Dill, Phys. Rev. A 6, 185 (1972).

²²U. Fano and J. Cooper, Rev. Mod. Phys. 40, 441 (1968).

²³J. C. Slater, Phys. Rev. 36, 57 (1930).

²⁴G. Basbas (unpublished).

²⁵E. Ehrhardt, M. Schulz, T. Tekaas, and K. Willmann, Phys. Rev. Letters 22, 89 (1969); H. Ehrhardt, K. H. Hesselbacher, K. Jung, M. Schulz, T. Tekaas, and K. Willmann, Z. Physik 244, 254 (1971).

²⁶W. K. Peterson, C. B. Opal, and E. C. Beaty, J. Phys. B 4, 1020 (1971).

²⁷L. H. Toburen, Phys. Rev. A 3, 216 (1971).

²⁸K. Omidvar, H. L. Kyle, and E. C. Sullivan, Phys. Rev. A 5, 1174 (1972).

²⁹G. Peach, J. Phys. B 4, 1670 (1971), and references therein.

³⁰H. Bethe, Z. Physik 76, 293 (1932).

³¹U. Fano, Phys. Rev. 95, 1198 (1954).

³²Y.-K. Kim and M. Inokuti, Phys. Rev. 175, 176 (1968).

³³M. Inokuti and Y.-K. Kim, Phys. Rev. 186, 100 (1969).

³⁴M. Inokuti, Argonne National Laboratory Report No. ANL-7220, 1966, p. 1 (unpublished).

³⁵Reference 2, Eq. (4.25).

³⁶S. T. Manson, Phys. Rev. A 5, 668 (1972).

³⁷V. V. Afrosimov, Yu. S. Gordeev, V. M. Lavrov, and S. G. Shchemelinin, Zh. Eksperim. i Teor. Fiz. 55, 1569 (1968) [Sov. Phys. JETP 28, 821 (1969)].

³⁸M. Ya. Amusia, N. A. Cherepkov, and S. I. Sheftel, Zh. Eksperim. i Teor. Fiz. 58, 618 (1970) [Sov. Phys. JETP 31, 332 (1970)].